

Realistic continuous-variable quantum teleportation with non-Gaussian resourcesF. Dell'Anno,^{1,2} S. De Siena,^{1,2} and F. Illuminati^{1,2,3,*}¹*Dipartimento di Matematica e Informatica, Università degli Studi di Salerno, Via Ponte don Melillo, I-84084 Fisciano, SA, Italy*²*CNR-INFM Coherently, Napoli, Italy, and CNISM and INFN Sezione di Napoli, Gruppo Collegato di Salerno, Baronissi, SA, Italy*³*ISI Foundation for Scientific Interchange, Viale Settimio Severo 65, I-00173 Torino, Italy*

(Received 14 October 2009; published 29 January 2010)

We present a comprehensive investigation of nonideal continuous-variable quantum teleportation implemented with entangled non-Gaussian resources. We discuss in a unified framework the main decoherence mechanisms, including imperfect Bell measurements and propagation of optical fields in lossy fibers, applying the formalism of the characteristic function. By exploiting appropriate displacement strategies, we compute analytically the success probability of teleportation for input coherent states and two classes of non-Gaussian entangled resources: two-mode squeezed Bell-like states (that include as particular cases photon-added and photon-subtracted de-Gaussified states), and two-mode squeezed catlike states. We discuss the optimization procedure on the free parameters of the non-Gaussian resources at fixed values of the squeezing and of the experimental quantities determining the inefficiencies of the nonideal protocol. It is found that non-Gaussian resources enhance significantly the efficiency of teleportation and are more robust against decoherence than the corresponding Gaussian ones. Partial information on the alphabet of input states allows further significant improvement in the performance of the nonideal teleportation protocol.

DOI: [10.1103/PhysRevA.81.012333](https://doi.org/10.1103/PhysRevA.81.012333)

PACS number(s): 03.67.Hk, 42.50.Ex, 42.50.Dv

I. INTRODUCTION

In recent years, theoretical and experimental investigation has been focused on the engineering of highly nonclassical, non-Gaussian states of the radiation field (for a review, see e.g., Ref. [1]). Interest in the production of non-Gaussian optical states is due to their strongly nonclassical properties, such as entanglement and negativity of the quasiprobability phase-space distributions, that are important for the efficient implementation of quantum information and communication protocols [1–5] and for quantum estimation tasks [6].

Several schemes for the generation of non-Gaussian states, both single-mode and two-mode, have already been proposed [7–13], and many successful and encouraging experimental realizations have been reported recently [14–19]. In principle, a very important result concerns the rigorous proof that various nonclassical properties are minimized by Gaussian states [20]. Therefore, it is reasonable to expect that the use of non-Gaussian resources may improve significantly the performance of quantum information protocols. In particular, concerning quantum teleportation with continuous variables (CV), it has been shown that the success probability of teleportation can be greatly increased by using entangled non-Gaussian resources in the framework of the ideal Braunstein-Kimble (BK) protocol [3,21–25].

Indeed, it has been shown that some specific two-mode non-Gaussian states, dubbed squeezed Bell-like states (that include as subcases photon-added and photon-subtracted de-Gaussified states [24]), when used as entangled resources provide a significant increase in the teleportation fidelity of single-mode input states under the ideal protocol [24]. Such an enhancement is due to a balancing of three different features [24]: the entanglement content of the resources, their

(appropriately defined) degree of affinity with the two-mode squeezed vacuum, and their (suitably measured) amount of non-Gaussianity. (For the precise definition of the last two quantities, see Refs. [24,26].) It has been suggested [24] that such states can be produced by combining simultaneous phase-matched multiphoton processes and conditional measurements.

The analysis of Ref. [24] has been extended to consider other classes of non-Gaussian resources, such as two-mode squeezed symmetric superpositions of Fock states and of squeezed catlike states, that allow high levels of performance in the teleportation of single-mode input states [27]. A partial preliminary analysis of nonideal cases has also been performed [27] by considering simple superpositions of independently generated fields converging on a common spatial volume, such as superpositions of a two-mode pure non-Gaussian resource and a two-mode thermal state [28]. In this elementary instance, mixed non-Gaussian entangled states remain preferred resources for teleportation when compared to mixed twin-beam Gaussian states [27].

In this work, using the formalism of the characteristic function, we study in full generality the BK protocol for CV teleportation in realistic conditions and with non-Gaussian entangled resources. We include in our investigation the main sources of decoherence that lead to the degradation of the transferred quantum information, such as losses due to imperfect homodyne measurements and damping due to the propagation of the optical fields in lossy fibers. The effects of these inefficiencies have already been considered, among others, in Refs. [29,30]. In particular Ref. [29] is concerned with the study of imperfect Bell measurements, whereas in Ref. [30] the authors investigate the limits of quantum teleportation due to photon absorption during propagation in fibers. Besides considering each problem separately, these and related works are always restricted to the use of Gaussian resources. The main object of the present work is to investigate the effect of the simultaneous presence of all sources of

*Corresponding author: illuminati@sa.infn.it

imperfection on the performance of CV teleportation protocols with non-Gaussian resources and their robustness against decoherence.

A general and exhaustive analysis turns out to be possible in the framework of the characteristic function representation. This method has been discussed in full generality for the description of ideal CV teleportation [31] and applied first to the case of Gaussian [31] and non-Gaussian resources [24,27]. We then extend the formalism to include the description of nonideal CV teleportation, including realistic Bell measurements and decoherence due to propagation in noisy channels. In order to investigate different optimization strategies of the nonideal protocol, we discuss optimization over the free parameters of the non-Gaussian resources as well as over the gain factor associated with the transmitted classical information [32] (for various strategies of gain tuning and of optimal gain, see also Refs. [30,33,34]). Indeed, in the instance of non-Gaussian resources, the gain can be considered as a further free parameter suitable for optimization.

The article is organized as follows. In Sec. II we extend the characteristic function formalism to include the case of realistic CV quantum teleportation. In Sec. III we introduce and discuss the main properties of some classes of non-Gaussian entangled resources. In Sec. IV we study the efficiency of the quantum teleportation protocol in the instance of fixed given values of the gain. In Sec. V we carry out an optimization procedure of the protocol over the entangled resources and the gain parameter. Finally, in Sec. VI we draw our conclusions and discuss some outlook on current and future research.

II. NONIDEAL CV TELEPORTATION PROTOCOL IN THE CHARACTERISTIC FUNCTION FORMALISM

In this section, we describe the realistic BK CV teleportation protocol in the formalism of the characteristic function. Although several alternative formalisms are available for the description of the BK CV teleportation protocol [35–40], the characteristic function representation proves to be particularly convenient when considering the nonideal case and non-Gaussian resources. The description of nonideal teleportation requires the introduction of mechanisms of loss and inefficiency in the main steps of the protocol. Indeed, a schematic description of the nonideal protocol is depicted in Fig. 1.

The input state and the entangled resource states are assumed to be initially pure. This is not a serious limitation because one can always map the case of a nonideal teleportation protocol with noisy (mixed) inputs and resources to an equivalent protocol with pure inputs and resources but with a correspondingly larger amount of noise affecting the protocol. A simple illustrative example of this equivalence is discussed later on in the present work.

The single-mode input state (*in*) is mixed to mode 1 of the entangled resource at a beam splitter. At the first user's (Alice) location, a Bell measurement, consisting in homodyne detections, is performed on the obtained state of mode "in" and mode 1. In order to describe a nonideal measurement, one needs to model/simulate the inefficiencies of the photodetectors. A realistic detector can be modeled by placing a fictitious beam splitter, that is, a partly transmitting

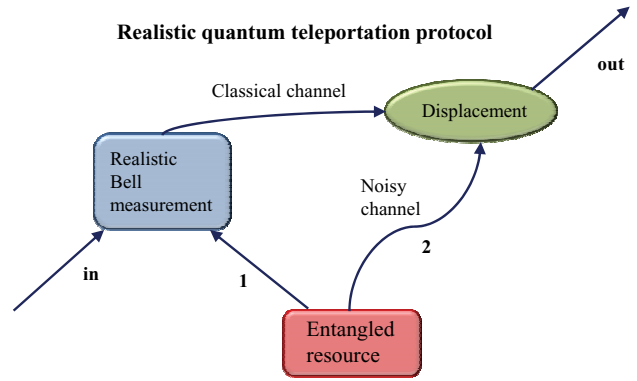


FIG. 1. (Color online) Pictorial representation of the nonideal BK CV quantum teleportation protocol. In the first step, the input mode is mixed by Alice with one of the two beams (modes) of the entangled resource; the ensuing state is then subject to a realistic Bell measurement. The result of the measure is communicated to Bob through a classical channel. In the second step, a unitary transformation, determined by the previous measurement, is applied to the second mode of the entangled resource, which is affected by decoherence during the propagation in a noisy channel, for example, a lossy fiber. The ensuing output state is the final teleported state.

mirror, in front of an ideal detector [41]. Based on such a prescription, a scheme describing a realistic Bell measurement is shown in Fig. 2.

After a realistic Bell measurement, the result is transmitted to the receiver (Bob) through a classical channel. The mode 2 of the entangled resource propagates in a noisy channel, as a lossy fiber, to Bob's location, where it undergoes a unitary displacement according to the result of the Bell measurement.

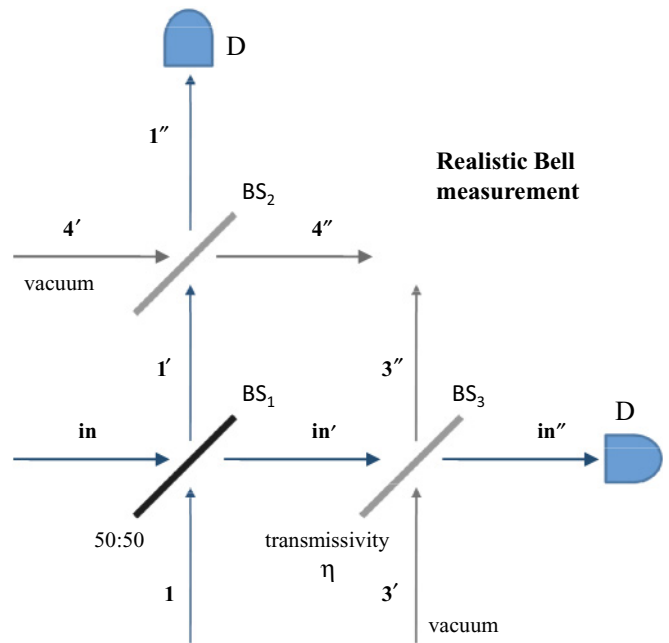


FIG. 2. (Color online) Model scheme of a realistic Bell measurement. The model takes into account the non-unity efficiency of the detectors *D* performing the homodyne measurement. In the depicted scheme, such inefficiency is simulated by the introduction of two fictitious beam splitters, BS₂ and BS₃, with equal transmissivity η .

It is important to note that the generation of the entangled resource can take place close to the sender, and typically very far away from the receiver, as one of the main tasks of quantum teleportation is the transfer of quantum information across long distances. It is then legitimate to assume that the radiation field associated with mode 1 is not affected by losses due to propagation, while the field associated with mode 2, which usually has to propagate over much longer distances, can be strongly affected by decoherence. The degradation of quantum information is caused by the propagation of field mode 2 in a noisy channel. Therefore, the output teleported state depends both on the inefficiency of the homodyne detectors and on the decoherence rate of the noisy channel.

We can formalize the effects of the previously described dynamics as follows. Let us denote by $\rho_{\text{in}} = |\phi\rangle_{\text{in}}\langle\phi|$ and $\rho_{\text{res}} = |\psi\rangle_{12}\langle\psi|$ the density matrices associated, respectively, with the single-mode pure input state and with the two-mode pure entangled resource. The single-mode input state is initially disentangled from the two-mode entangled resource, so that the the initial three-mode field is $\rho_0 = \rho_{\text{in}} \otimes \rho_{\text{res}}$, and the initial global characteristic function reads

$$\begin{aligned} \chi_0(\alpha_{\text{in}}; \alpha_1; \alpha_2) &= \text{Tr}[\rho_0 D_{\text{in}}(\alpha_{\text{in}}) D_1(\alpha_1) D_2(\alpha_2)] \\ &= \chi_{\text{in}}(\alpha_{\text{in}}) \chi_{\text{res}}(\alpha_1; \alpha_2), \end{aligned} \quad (1)$$

where Tr denotes the trace operation, $D_j(\alpha_j)$ denotes the displacement operator for the mode j ($j = \text{in}, 1, 2$), χ_{in} is the characteristic function of the input state, and χ_{res} is the characteristic function of the entangled resource. By defining the quadrature operators $X_j = \frac{1}{\sqrt{2}}(a_j + a_j^\dagger)$ and $P_j = \frac{i}{\sqrt{2}}(a_j^\dagger - a_j)$ ($j = \text{in}, 1, 2$) and the associated phase-space real variables $x_j = \frac{1}{\sqrt{2}}(\alpha_j + \alpha_j^*)$ and $p_j = \frac{i}{\sqrt{2}}(\alpha_j^* - \alpha_j)$, the characteristic function can be written in terms of x_j, p_j ; that is, $\chi_0(\alpha_{\text{in}}; \alpha_1; \alpha_2) \equiv \chi_0(x_{\text{in}}, p_{\text{in}}; x_1, p_1; x_2, p_2)$.

The first step of the protocol consists of the Bell measurement at Alice's location, that is, the homodyne measurements of the first quadrature of the mode 1 and of the second quadrature of the mode in , with results \tilde{x} and \tilde{p} , respectively. After such nonideal Bell measurement (BM), the remaining mode 2 is left in a mixed state described by the corresponding single-mode characteristic function $\chi_{\text{Bm}}(x_2, p_2)$. In Appendix A we prove in detail how to compute it in full generality for arbitrary single-mode inputs and arbitrary two-mode entangled resources. Here we report only the final expression:

$$\begin{aligned} \chi_{\text{Bm}}(x_2, p_2) &= \frac{\mathcal{P}^{-1}(\tilde{p}, \tilde{x})}{(2\pi)^2} \int d\xi d\nu e^{i\xi\tilde{p} - i\tilde{x}\nu} \\ &\times \chi_{\text{in}}\left(\frac{T\xi}{\sqrt{2}}, \frac{T\nu}{\sqrt{2}}\right) \chi_{\text{res}}\left(\frac{T\xi}{\sqrt{2}}, -\frac{T\nu}{\sqrt{2}}; x_2, p_2\right) \\ &\times \exp\left[-\frac{R^2}{4}(\xi^2 + \nu^2)\right], \end{aligned} \quad (2)$$

where T^2 and $R^2 = (1 - T^2)$ denote, respectively, the transmissivity and reflectivity of the beam splitters that model the losses. The function $\mathcal{P}(\tilde{p}, \tilde{x})$ is the distribution of the measurement outcomes \tilde{p} and \tilde{x} (see Appendix A). Note that the Gaussian exponential in Eq. (2) is related to the vacua entering the input ports of the fictitious beam splitters.

Afterwards, mode 2 propagates in a damping channel, like, e.g., a lossy fiber, before it reaches Bob's location. The Markovian dynamics of a system subject to damping is described, in the interaction picture, by the following master equation for the density operator ρ [42,43]:

$$\partial_t \rho = \frac{\Upsilon}{2} \{n_{\text{th}} L[a_2^\dagger] \rho + (n_{\text{th}} + 1) L[a_2] \rho\}, \quad (3)$$

where the Lindblad superoperators are defined as $L[\mathcal{O}]\rho \equiv 2\mathcal{O}\rho\mathcal{O}^\dagger - \mathcal{O}^\dagger\mathcal{O}\rho - \rho\mathcal{O}^\dagger\mathcal{O}$, Υ is the mode damping rate, and n_{th} is the number of thermal photons. Finally, at Bob's location, a displacement $\lambda = g(\tilde{x} + i\tilde{p})$ is performed on mode 2. The real parameter g is the so-called gain factor [40]. The combined effect of propagation in a damping channel and unitary displacement determines the characteristic function $\chi_{\text{out}}(x_2, p_2)$ of the final output state of the teleportation protocol (see Appendix A for details):

$$\begin{aligned} \chi_{\text{out}}(x_2, p_2) &= \chi_{\text{in}}(gT x_2, gT p_2) \\ &\times \chi_{\text{res}}(gT x_2, -gT p_2; e^{-\frac{\tau}{2}} x_2, e^{-\frac{\tau}{2}} p_2) \\ &\times \exp\left[-\frac{1}{2}\Gamma_{\tau,R}(x_2^2 + p_2^2)\right], \end{aligned} \quad (4)$$

where $\tau = \Upsilon t$, and the thermal "renormalized" phase-space covariance $\Gamma_{\tau,R}$ is defined as

$$\Gamma_{\tau,R} = (1 - e^{-\tau})\left(\frac{1}{2} + n_{\text{th}}\right) + g^2 R^2. \quad (5)$$

The form of Eq. (4) highlights the different roles played by the two sources of noise introduced in the teleportation protocol, associated, respectively, with the damping rate Υ and the reflectivity R^2 . The two decoherence mechanisms act separately but also in combination, as one can see from the Gaussian exponential factor in Eq. (4), which in fact is nonvanishing for $R \neq 0$ and/or $\tau \neq 0$. The effect of the imperfect Bell measurement is expressed also by the presence of the scale factor T in the arguments of the input and resource characteristic functions χ_{in} and χ_{res} . Vice versa, decoherence due to noisy propagation affects obviously only mode 2 by means of the exponentially decreasing weight $e^{-\frac{\tau}{2}}$ in the arguments of χ_{res} . The factorized form of the output characteristic function, holding for the ideal protocol [31],

$$\chi_{\text{out}}(x_2, p_2) = \chi_{\text{in}}(x_2, p_2) \chi_{\text{res}}(x_2, -p_2; x_2, p_2), \quad (6)$$

is recovered, as expected, from Eq. (4) when $R = 0$ ($T = 1$), $\Upsilon = 0$ ($\tau = 0$), and $g = 1$.

III. ENTANGLED RESOURCES: TWO CLASSES OF OPTIMIZED NON-GAUSSIAN STATES

Given the general description of the nonideal protocol in terms of the characteristic functions, in this section we analyze the performance of two classes of non-Gaussian entangled resources for the teleportation of input coherent states, respectively, the two-mode squeezed Bell-like states $|\psi\rangle_{\text{SB}}$ and the two-mode squeezed catlike states $|\psi\rangle_{\text{SC}}$:

$$|\psi\rangle_{\text{SB}} = S_{12}(\zeta)\{\cos\delta|0, 0\rangle + e^{i\theta}\sin\delta|1, 1\rangle\}, \quad (7)$$

$$|\psi\rangle_{\text{SC}} = \mathcal{N}_{\text{SC}} S_{12}(\zeta)\{\cos\delta|0, 0\rangle + e^{i\theta}\sin\delta|\gamma, \gamma\rangle\}, \quad (8)$$

where $S_{12}(\zeta) = e^{-\zeta a_1^\dagger a_2^\dagger + \zeta a_1 a_2}$ is the two-mode squeezing operator, $\zeta = r e^{i\phi}$, $|m, n\rangle \equiv |m\rangle_1 \otimes |n\rangle_2$ is a two-mode Fock

state (of modes 1 and 2), $|\gamma, \gamma\rangle \equiv |\gamma\rangle_1 \otimes |\gamma\rangle_2$ is a symmetric two-mode coherent state with complex amplitude $\gamma = |\gamma|e^{i\varphi}$, and the normalization factor \mathcal{N}_{SC} is $\mathcal{N}_{\text{SC}} = \{1 + e^{-|\gamma|^2} \sin 2\delta \cos \theta\}^{-1/2}$. In order to obtain a maximization of the teleportation fidelity, it is necessary to perform a simultaneous balanced optimization, on the free parameters (δ, θ, γ) , of some partially competing properties [24,27]. These include the entanglement content, the amount of non-Gaussianity of the state [26], and a squeezed vacuum affinity \mathcal{G} . For a generic pure state $|\psi\rangle$, the latter is defined as [24,27]

$$\mathcal{G} = \sup_r |(-r|\psi\rangle)|^2, \quad (9)$$

with $| -r\rangle = S_{12}(-r)|0, 0\rangle$. Indeed, the optimal non-Gaussian resources (7) and (8) exhibit a sufficient squeezed vacuum affinity, which then appears to be a crucially needed property in order to select efficient and highly performing non-Gaussian resources. For instance, one could as well consider a different form of the squeezed Bell-like state, the so-called ‘‘Buridan donkey’’ or ‘‘Hamlet’’ state $|\psi\rangle_{\text{SB2}}$, that is obtained from the singlet Bell state as follows:

$$|\psi\rangle_{\text{SB2}} = S_{12}(\zeta)\{\cos \delta|0, 1\rangle + e^{i\theta} \sin \delta|1, 0\rangle\}. \quad (10)$$

It is indeed simple to verify that, although such a state, at fixed squeezing, is more entangled than a Gaussian twin beam, it performs less efficiently both in the ideal and in the realistic teleportation protocol. This fact can be understood if one looks at the behavior of the squeezed vacuum affinity [24]. Namely, the Buridan donkey state, Eq. (10), does not contain the fundamental Gaussian contribution coming from the squeezed vacuum. Therefore, it is ‘‘unbalanced,’’ in the sense that it is less affine to the squeezed vacuum, and excessively non-Gaussian compared to the optimized Bell-like state $|\psi\rangle_{\text{SB}}$. Therefore, the fine interplay among these three quantities, that is, the entanglement, the degree of non-Gaussianity, and, in particular, the squeezed vacuum affinity, cannot be realized in the non-Gaussian resource (10) [24]. The crucial role played by the squeezed vacuum affinity for the performance of different non-Gaussian resources has been studied in Ref. [27]. In particular, it has been shown that, in the ideal teleportation protocol, the two-mode squeezed symmetric superposition of Fock states, that is, $S_{12}(\zeta) \sum_{k=0}^2 c_k |k, k\rangle$, when optimized for the teleportation of both input coherent states and single-photon states, reduces to a squeezed truncated twin beam, that is, $S_{12}(-r) \sum_{k=0}^2 \tanh^k s |k, k\rangle$. In the same article, it has been also shown that, in the ideal teleportation protocol, the optimized two-mode squeezed catlike states, that is, Eq. (8), possess a high amount of squeezed vacuum affinity. Therefore, besides a certain amount of entanglement, also a sufficient degree of squeezed vacuum affinity appears to be necessary for a non-Gaussian resource to be optimal for a BK teleportation protocol.

Clearly, the performance of BK teleportation protocols depends strongly on the structure of the second-order correlations in the entangled resources. In this sense the BK protocol, with its structure of homodyne measurements, is particularly tailored to the use of Gaussian resources. Therefore, a non-Gaussian resource may improve on the performance of a corresponding Gaussian one only if the fundamental Gaussian contribution coming from the squeezed

vacuum is subject to a not too drastic modification. A large value of the affinity assures that the non-Gaussian resource satisfies such a requirement. The interplay of the affinity with the non-Gaussianity and the degree of entanglement allows one to single out those non-Gaussian resources possessing higher-order correlations that add to the leading Gaussian structure of the two-mode entangled resource, thus enhancing further the protocol efficiency, and lacking those non-Gaussian contributions that are incompatible with the structure of the BK protocol.

Indeed, a very interesting question open for future investigation is the inverse of the one studied in the present article. Here we are analyzing the problem of optimizing non-Gaussian resources given the BK protocol. The inverse question would be that of adapting the protocol to the resources. Namely, given a certain class of non-Gaussian squeezed resources with some given properties, one asks how the BK protocol would have to be modified in order to optimize the fidelity of teleportation.

We now proceed to determine the general expression of the fidelity of teleportation in terms of the characteristic function for the three different non-Gaussian entangled resources $|\psi\rangle_{\text{SB}}$, $|\psi\rangle_{\text{SC}}$, and $|\psi\rangle_{\text{SB2}}$. For instance, the two-mode characteristic function χ_{SB} of the entangled resource (7) reads

$$\chi_{\text{SB}}(\alpha_1, \alpha_2) = \text{Tr}[|\psi\rangle_{\text{SB}} \langle\psi| D_1(\alpha_1) D_2(\alpha_2)], \quad (11)$$

and analogous expressions hold for χ_{SC} and χ_{SB2} . The corresponding explicit expression is obtained using the two-mode Bogoliubov transformations

$$S_{12}^\dagger(\zeta) a_i S_{12}(\zeta) = (\cosh r) a_i - e^{i\phi} (\sinh r) a_j^\dagger, \quad (12)$$

$$(i \neq j = 1, 2),$$

and the relation

$$\langle m|D(\alpha)|n\rangle = \left(\frac{n!}{m!}\right)^{1/2} \alpha^{m-n} e^{-\frac{1}{2}|\alpha|^2} L_n^{(m-n)}(|\alpha|^2), \quad (13)$$

where $L_n^{(m-n)}(\cdot)$ denotes the associated Laguerre polynomial of order n .

The quantity measuring the success probability of a teleportation protocol is the fidelity of teleportation $\mathcal{F} = \text{Tr}[\rho_{\text{in}}\rho_{\text{out}}]$. In the formalism of the characteristic function, the fidelity reads

$$\mathcal{F} = \frac{1}{\pi} \int d^2\alpha \chi_{\text{in}}(\alpha) \chi_{\text{out}}(-\alpha),$$

$$= \frac{1}{2\pi} \int dx_2 dp_2 \chi_{\text{in}}(x_2, p_2) \chi_{\text{out}}(-x_2, -p_2), \quad (14)$$

where $\alpha = \frac{1}{\sqrt{2}}(x_2 + ip_2)$, $d^2\alpha = \frac{1}{2}dx_2 dp_2$, and $\chi_{\text{out}}(\alpha) \equiv \chi_{\text{out}}(x_2, p_2)$ is given by Eq. (4). In the case of input coherent states $\rho_{\text{in}} = |\beta\rangle_{\text{in}} \langle\beta|$ with complex amplitude β , which we will always consider in the following, the characteristic function of the input $\chi_{\text{in}}(\alpha)$ reads

$$\chi_{\text{in}}(\alpha) = e^{-\frac{1}{2}|\alpha|^2 + (\alpha\beta^* - \alpha^*\beta)}. \quad (15)$$

Eq. (14) is the fundamental quantity that measures the efficiency of a CV teleportation protocol (ideal or nonideal). At fixed squeezing, the optimization procedure consists of the maximization of the teleportation fidelity (14) over the free parameters of the non-Gaussian entangled resources,

Eqs. (7), (8), and (10). Since it can be verified explicitly that the optimal choice for the phases ϕ , θ , and φ are $\phi = \pi$ and $\theta = \varphi = 0$, the squeezed Bell-like state $|\psi_{\text{SB}}\rangle$ and the Buridan donkey state $|\psi_{\text{SB}2}\rangle$ have a unique available free parameter δ . On the other hand, the squeezed catlike state $|\psi_{\text{SC}}\rangle$ has two free parameters, the angle δ and the modulus $|\gamma|$. The analytical expressions of the teleportation fidelities of input coherent states corresponding to the three different classes of non-Gaussian resources, respectively, $\mathcal{F}_{\text{SB}}^{(g)}(r, \delta)$, $\mathcal{F}_{\text{SC}}^{(g)}(r, \delta, |\gamma|)$, and $\mathcal{F}_{\text{SB}2}^{(g)}(r, \delta)$, are reported in Appendix C, Eqs. (C1), (C4), and (C6). Let us notice that we have introduced the superscript (g) to explicitly indicate the dependence on the gain g . It is simple to verify that, for arbitrary g , the fidelities are explicitly dependent on the amplitude β of the input coherent states. In the next sections, the (numerical) optimization procedures of the fidelity \mathcal{F} are implemented following two different routes. In Sec. IV we operate at a specific value of the gain $g = 1/T$, for a fixed value of the transmissivity T^2 . This is the only choice that makes the fidelity independent of β . In Sec. V we adopt a more general approach by letting g be a fully free parameter and performing appropriate optimization procedures.

In both cases, the maximization is carried out at fixed (finite) squeezing r and at fixed τ , n_{th} , and R . From an operational point of view, fixing these parameters is equivalent to assuming control of the characteristics of the experimental apparatus, including the inefficiency of the photodetectors and the length and damping rate of the noisy channel. Finally, concerning the experimental realization of the two-mode non-Gaussian resources, Eqs. (7) and (8), a detailed theoretical proposal is put forward in Ref. [24]. The experimental realization of the single-mode version of the state $|\psi\rangle_{\text{SC}}$ has been reported in Ref. [19].

IV. β -INDEPENDENT OPTIMAL FIDELITY

In this section, we analyze the success probability of quantum teleportation for the gain g fixed to be $g = 1/T$. It is immediate to verify that with this choice, the fidelity becomes β independent (see Appendix C). This choice allows us to assume no knowledge about the alphabet of input coherent states, whereas in the next section we assume a partial knowledge of the input states over an interval of values of β . For $g = 1/T$, the expressions for the fidelities $\mathcal{F}_{\text{SB}}(r, \delta)$, $\mathcal{F}_{\text{SC}}(r, \delta, |\gamma|)$, and $\mathcal{F}_{\text{SB}2}(r, \delta)$ (where the superscript (g) has been removed) greatly simplify. At fixed r , τ , n_{th} , and R , the optimal fidelities of teleportation are defined as

$$\mathcal{F}_{\text{opt}}^{(\text{SB})} = \max_{\delta} \mathcal{F}_{\text{SB}}(r, \delta), \quad (16)$$

$$\mathcal{F}_{\text{opt}}^{(\text{SB}2)} = \max_{\delta} \mathcal{F}_{\text{SB}2}(r, \delta), \quad (17)$$

$$\mathcal{F}_{\text{opt}}^{(\text{SC})} = \max_{\delta, |\gamma|} \mathcal{F}_{\text{SC}}(r, \delta, |\gamma|). \quad (18)$$

In Fig. 3 we plot the optimal fidelities, corresponding to the three classes of non-Gaussian resources, as functions of the squeezing parameter r at different values of the parameters τ , n_{th} , and $R = \sqrt{1 - T^2}$. For comparison, the fidelity associated with the Gaussian squeezed vacuum (twin beam) is reported as well. In order to understand the separate effects of the

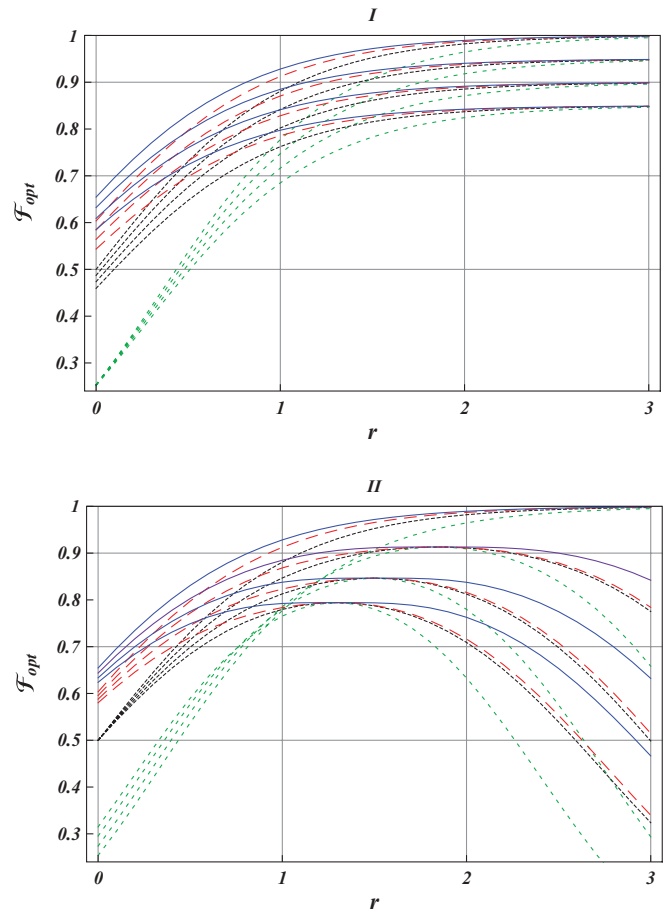


FIG. 3. (Color online) Optimal fidelities of teleportation \mathcal{F}_{opt} as functions of the squeezing parameter r , for different values of the parameters τ , n_{th} , and R . The fidelities correspond to the teleportation of single-mode input coherent states $|\beta\rangle$ using two-mode squeezed Bell-like states (solid line) or two-mode squeezed catlike states (dashed line) as entangled resources. The fidelities associated with the two-mode squeezed vacuum (dotted line) and with the Buridan donkey states (wide-spaced dotted line) are reported for comparison. In panel I, $\tau = 0$, $n_{\text{th}} = 0$, and the reflectivity is fixed at the values $R^2 = 0, 0.05, 0.1, 0.15$. For each entangled resource (associated with a specific plot style), the corresponding curves are ordered from top to bottom with increasing R^2 . In panel II, $n_{\text{th}} = 0$, $R = 0$, and the reduced time is fixed at the values $\tau = 0, 0.1, 0.2, 0.3$. For each entangled resource (associated with a specific plot style) the corresponding curves are ordered from top to bottom with increasing τ .

two different sources of decoherence on the degradation of the fidelity, we consider two cases: (i) decoherence due to imperfect Bell measurements alone, that is, $R > 0$ and $\tau = 0$ (see Fig. 3, panel I); and (ii) decoherence due to propagation in noisy channels alone, that is, $R = 0$ and $\tau > 0$ (see Fig. 3, panel II).

In the first case, the fidelities grow monotonically, with increasing r , tending toward an asymptotic saturation value. This behavior is equivalent to that observed in the instance of an ideal protocol with noisy resources [27]. Indeed, the case of a nonideal teleportation protocol with noisy (mixed) resources is equivalent to the case of a nonideal protocol with pure resources but with a larger amount of noise.

In the second case, as r increases, the fidelity first increases up to a τ -dependent maximum, $r_{\max}(\tau)$, and then decreases for larger values of r . This behavior can be explained observing that there are two competing effects associated to increasing the degree of squeezing. The first effect is constructive and is due to the enhanced affinity of the entangled resource with an Einstein-Podolsky-Rosen (EPR) state for increasing r . This constructive effect is contrasted by a disruptive one due to the optical photons generated by the squeezing that add to the thermal photons of the channel (initially set to zero). For not too large values of r , the first effect dominates, until a maximum is reached at $r = r_{\max}(\tau)$. For $r > r_{\max}(\tau)$ the disruptive effect becomes dominant, and the increasingly large number of optical photons amplifies the decoherence, leading to a strong suppression of the fidelity. The interplay between squeezing r and channel decay rate τ can be understood quantitatively by investigating the structure of the output characteristic function χ_{out} , Eq. (4), that enters in the expression of the fidelity (14). For $gT = 1$, χ_{out} takes the form

$$\begin{aligned} \chi_{\text{out}}(x_2, p_2) &= e^{-\frac{1}{2}\Gamma_{\tau,R}(x_2^2+p_2^2)} \chi_{\text{in}}(x_2, p_2) \\ &\quad \times \chi_{\text{res}}(x_2, -p_2; e^{-\frac{\tau}{2}}x_2, e^{-\frac{\tau}{2}}p_2), \end{aligned}$$

where $\Gamma_{\tau,R}$ is given by Eq. (5). We see that, if $\tau \neq 0$, the exponential weights $e^{-\tau/2}$ introduce an asymmetry between the two modes of the resource in the expression of the characteristic function χ_{res} . This asymmetry is responsible for the decrease of the fidelity for $r > r_{\max}(\tau)$ at $\tau \neq 0$. The important ensuing conclusion is that it is in fact detrimental to increase the squeezing too much when the losses cannot be reduced strongly. Therefore, the primary experimental goal should always be that of reducing the losses rather than incrementing the squeezing.

Moreover, Fig. 3 (panel II) shows that indeed at current experimentally attainable values of the squeezing, that is, $r \lesssim 1.5$, the nonideal teleportation protocol operates already in the regime of best efficiency, and both the squeezed Bell-like resources (7) and the squeezed catlike resources (8) perform much better than the corresponding (that is, at the same squeezing) Gaussian resources. This result generalizes and confirms the analogous behavior observed in the instance of ideal protocols [24,27]. On the contrary, as already anticipated in the previous section, the Buridan donkey resources allow for teleportation fidelities even worse than those associated with the Gaussian twin beam. Indeed, from Eq. (C6) it follows that the optimal β -independent fidelity $\mathcal{F}_{\text{opt}}^{(\text{SB}2)}$ is obtained (with $g = 1/T$) by letting $\delta = 0$. In this case, the Buridan donkey state trivially reduces to a two-mode squeezed Fock state.

It is worth noting that, at $gT = 1$ and any fixed value of τ , all the non-Gaussian resources share with the Gaussian one the same maximum value of the fidelity, obtained at the same value $r_{\max}(\tau)$ of the squeezing parameter. This implies that, at given τ , one can determine the value $r_{\max}(\tau)$ for all the various resources by just considering the simple Gaussian instance. A straightforward computation then yields

$$\exp\{2r_{\max}\} = \sqrt{\frac{\cosh(\tau/2) + 1}{\cosh(\tau/2) - 1}}. \quad (19)$$

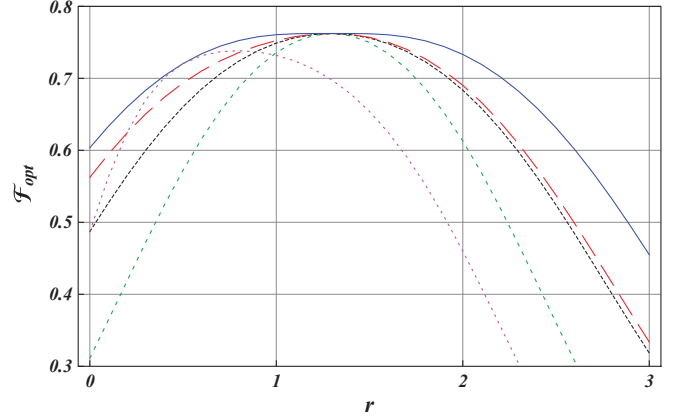


FIG. 4. (Color online) Optimal fidelities of teleportation \mathcal{F}_{opt} as functions of the squeezing parameter r , with $\tau = 0.3$, $n_{\text{th}} = 0$, and $R^2 = 0.05$. The different lines represent the fidelity of teleportation of input coherent states $|\beta\rangle$, corresponding, respectively, to the following entangled resources: squeezed Bell-like state (solid line), squeezed catlike state (dashed line), squeezed vacuum (dotted line), Buridan donkey state (wide-spaced dotted line), and photon-subtracted squeezed state (dot-dashed line).

We see that, for increasing τ , the range $[0, r_{\max}(\tau)]$ of best efficiency reduces.

Finally, we consider the combined effect of the two decoherence mechanisms. In Fig. 4 we plot the optimal fidelities associated with the different classes of non-Gaussian resources with the experimental parameters fixed at the values $\tau = 0.3$, $n_{\text{th}} = 0$, and $R^2 = 0.05$. In this case, the simultaneous presence of the two effects leads to a strong suppression of the fidelity both with respect to the ideal case and to each of the two nonideal cases taken separately. A regime of best efficiency is still present, but significantly reduced.

In Fig. 4, we also report the fidelity of teleportation associated with the two-mode photon-subtracted squeezed states:

$$\begin{aligned} |\psi\rangle_{\text{PSS}} &= \mathcal{N} a_1 a_2 S_{12}(\zeta) |0, 0\rangle \\ &= \mathcal{N} e^{i\phi} S_{12}(\zeta) \{-|0, 0\rangle + e^{i\phi} \tanh r |1, 1\rangle\}, \quad (20) \end{aligned}$$

where $\mathcal{N} = (1 + \tanh^2 r)^{-1/2}$ is the normalization [24]. This non-Gaussian resource belongs, as a particular subcase, to the class of the squeezed Bell-like resources. Indeed, Eq. (7) reduces to Eq. (20) for $\delta = \arctan(\tanh r)$ (with $\phi = \pi$ and $\theta = 0$). The interest in the resources (20) is due to the fact that such states have already been produced in the laboratory [16,17]. Furthermore, the corresponding de-Gaussification scheme can be easily integrated in the BK teleportation protocol [21]. As in the ideal instance [24], and also in the realistic case, see Fig. 4, the performance of the non-Gaussian resource (20) is intermediate between that of the Gaussian twin beam and that of the squeezed Bell-like states for $0 \leq r \lesssim 1$, whereas for $r \gtrsim 1$ it degrades much faster. The affinity to the two-mode squeezed vacuum of state (20) decreases for growing r ; correspondingly, the resource becomes more and more non-Gaussian. Moreover, for some intervals of values of the squeezing parameter the photon-subtracted squeezed states behave better than the squeezed catlike states. It is worth noticing that there exists a “crossing” value of r at

which the optimal squeezed Bell-like state reduces to the photon-subtracted squeezed state and thus the corresponding fidelities of teleportation coincide (see Fig. 4).

In this section we have considered always the case $gT = 1$. The scenario changes dramatically if $gT \neq 1$. Indeed, in this case the analytical expressions of the fidelities (C1), (C4), (C5), and (C6) depend on the coherent amplitude β . This dependence affects quite significantly the behavior of the fidelities as we will see in the next section.

V. AVERAGE OPTIMAL FIDELITY AND ONE-SHOT FIDELITY

In order to investigate possible improvements in the efficiency of the teleportation protocol, in this section we aim at optimizing the success probability of teleportation assuming g as a further free optimization parameter. The fidelity of teleportation as a function of the gain is studied for several input states in Ref. [33], while displacement strategies are considered in Ref. [34], in order to improve the output quality for a reduced alphabet of possible input states. These two important works are concerned with the study of the ideal protocol implemented using Gaussian resources. The effect of absorption due to propagation in fibers is studied in Ref. [30], where, for the case of Gaussian resources, it is shown that the gain-optimized fidelity of teleportation is strongly suppressed.

Let us now describe the optimization procedure applied to the instance of non-Gaussian resources. Following the approach of Refs. [30,34], we define the average fidelity $\overline{\mathcal{F}}$ by averaging the β -dependent fidelity $\mathcal{F}(\beta)$ over the set of input coherent states $|\beta\rangle$ as follows:

$$\overline{\mathcal{F}} = \int d^2\beta \mathcal{F}(\beta) p(\beta), \quad (21)$$

$$p(\beta) = (\pi\sigma)^{-1} \exp\{-\sigma^{-1} |\beta|^2\}, \quad (22)$$

where the function $p(\beta)$ (22) is a Gaussian distribution centered at $\beta = 0$. The variance parameter σ determines the cutoff of the amplitude β and thus the reduced alphabet that one considers. We compare our results with the quantum benchmark for the storage and transmission of coherent states distributed according to Eq. (22) [44]. This benchmark is equivalent to the upper bound $\mathcal{F}_{\text{class}}$ achievable with any classical strategy and satisfying the inequality [44]

$$\mathcal{F}_{\text{class}} \leq \frac{\sigma + 1}{2\sigma + 1}. \quad (23)$$

The first step of our optimization procedure, employing Eqs. (C1) and (C4), is to determine the average fidelities $\overline{\mathcal{F}}_{\text{SB}}^{(g)}(r, \delta)$ and $\overline{\mathcal{F}}_{\text{SC}}^{(g)}(r, \delta, |\gamma|)$, whose expressions we do not report because their long and cumbersome structure is not particularly illuminating. Further, we do not apply the optimization procedure to the teleportation fidelity associated with the Buridan donkey resource as we have already showed that no enhancement can be obtained compared to the Gaussian twin beam resource. At fixed squeezing r and experimental parameters τ , n_{th} , and R , we define the optimal values g_{opt} , δ_{opt} , and $|\gamma_{\text{opt}}|$ of the free parameters as those that maximize the fidelities averaged over the values of β weighted according

to the normal distribution $p(\beta)$ (22):

$$\overline{\mathcal{F}}_{\text{SB}}^{(g, \text{opt})}(r, \delta_{\text{opt}}) \doteq \max_{\{g, \delta\}} \overline{\mathcal{F}}_{\text{SB}}^{(g)}(r, \delta), \quad (24)$$

$$\overline{\mathcal{F}}_{\text{SC}}^{(g, \text{opt})}(r, \delta_{\text{opt}}, |\gamma_{\text{opt}}|) \doteq \max_{\{g, \delta, |\gamma|\}} \overline{\mathcal{F}}_{\text{SC}}^{(g)}(r, \delta, |\gamma|). \quad (25)$$

The optimal values of the parameters are determined numerically. Next, we introduce the one-shot fidelities \mathcal{F}_{1s} as the nonaveraged fidelities evaluated at the optimal values of the parameters and a fixed value of β :

$$\mathcal{F}_{1s}^{(\text{SB})}(\beta, r) \doteq \mathcal{F}_{\text{SB}}^{(g, \text{opt})}(\beta, r, \delta_{\text{opt}}), \quad (26)$$

$$\mathcal{F}_{1s}^{(\text{SC})}(\beta, r) \doteq \mathcal{F}_{\text{SC}}^{(g, \text{opt})}(\beta, r, \delta_{\text{opt}}, |\gamma_{\text{opt}}|). \quad (27)$$

For each possible value of β one can estimate the success probability of teleportation associated with a specific event. The functions $\mathcal{F}_{1s}(\beta, r)$ yield the teleportation fidelities at given squeezing r and for an input coherent state with specific amplitude β . Partial information about the alphabet of input states, quantified by the choice of the variance σ in the distribution (22), can be exploited to obtain a refinement of the optimization procedure. Indeed, we expect that smaller values of σ , corresponding to a better knowledge of the alphabet of input states, will lead to higher values of the one-shot fidelities.

A. Fidelities: Variable r , fixed τ

In Fig. 5, at the same fixed parameters of Fig. 4, $\tau = 0.3$, $n_{\text{th}} \approx 0$, $R^2 = 0.05$, we plot the one-shot fidelity \mathcal{F}_{1s} as a function of r , both for the non-Gaussian resources and for the Gaussian twin beam. In panel I we plot the one-shot fidelities for $\sigma = 10$ and $\beta = 1, 2, 3$; in panel II we plot the one-shot fidelities for $\sigma = 100$ and $\beta = 3, 5, 10$ (obviously $|\beta|^2$ must fall in the interval $[0, \sigma]$). Let us notice that according to Eq. (23), the quantum benchmarks for the two choices of σ are $\mathcal{F}_{\text{class}}(\sigma = 10) \approx 0.523$ and $\mathcal{F}_{\text{class}}(\sigma = 100) \approx 0.502$.

Panel I of Fig. 5, corresponding to $\sigma = 10$ and small values of $|\beta|$, shows that, as soon as r is different from zero, all the resources yield fidelities above the quantum benchmark. Moreover, one observes a significant enhancement of the fidelities with respect to the β -independent ones of Fig. 4 (corresponding to $g = 1/T$). Indeed, while the β -independent fidelities in Fig. 4 are well below the value 0.8, all the one-shot fidelities of panel I of Fig. 5 lie above this value for squeezing r ranging from about 0.8 to about 1.2, depending on the resource being considered. Also in this case the non-Gaussian resources exhibit better performances with respect to the Gaussian ones. Panel II of Fig. 5 shows that for $\sigma = 100$ and larger values of $|\beta|$, the enhancement of the fidelity is quite modest compared to the β -independent fidelity, reported in Fig. 4. This result is not surprising because a variance $\sigma = 100$ obviously allows less knowledge of the alphabet of input states with respect to the case $\sigma = 10$. It is important to remark that the curves corresponding to the same entangled resource but different values of β become effectively distinguishable only when $r \gtrsim 1$.

B. Fidelities: Variable τ , fixed r

We now study the fidelities as functions of the reduced time, or effective length of the fiber τ , at fixed squeezing r . To this

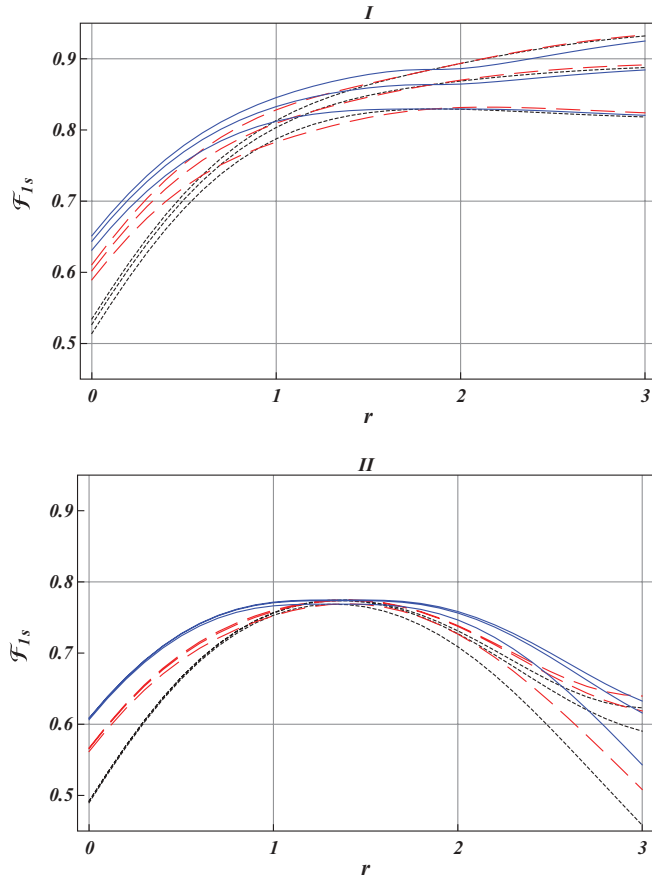


FIG. 5. (Color online) One-shot fidelity of teleportation \mathcal{F}_{1s} , for input coherent states $|\beta\rangle$, as a function of the squeezing parameter r , with $\tau = 0.3$, $n_{th} = 0$, $R^2 = 0.05$, for the following resources: squeezed Bell-like state (solid line), squeezed catlike state (dashed line), and a squeezed vacuum (dotted line). In panel I, $\beta = 1, 2, 3$ and $\sigma = 10$. In panel II, $\beta = 3, 5, 10$ and $\sigma = 100$. For each entangled resource (associated with a specific plot style), the corresponding curves are ordered from top to bottom with increasing β .

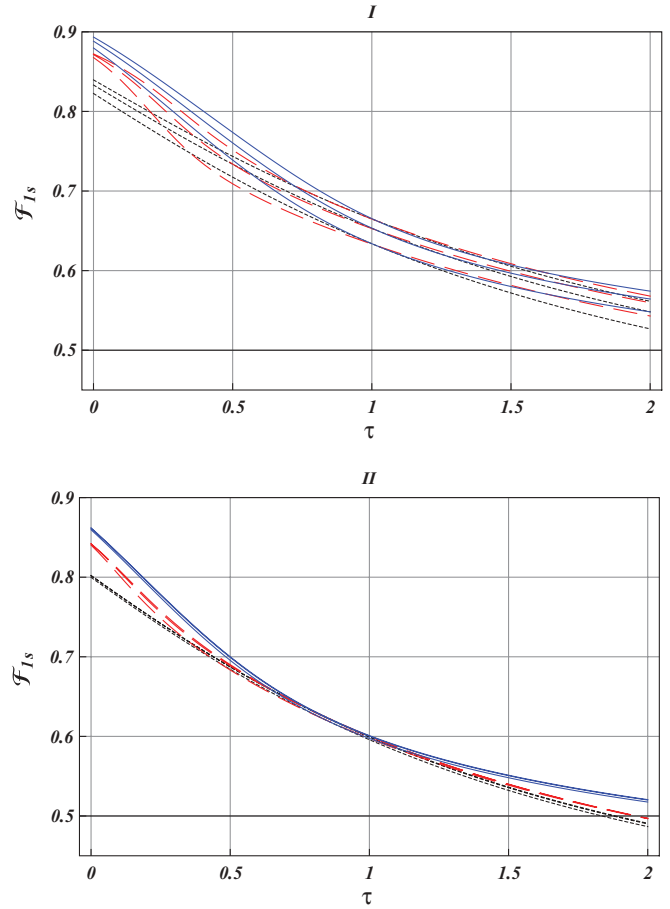


FIG. 6. (Color online) One-shot fidelity of teleportation \mathcal{F}_{1s} , for input coherent states $|\beta\rangle$, as a function of the reduced time τ , with $r = 0.8$, $n_{th} = 0$, $R^2 = 0.05$, for the following entangled resources: squeezed Bell-like state (solid line), squeezed catlike state (dashed line), and squeezed vacuum (dotted line). In panel I, $\beta = 1, 2, 3$ and $\sigma = 10$. In panel II, $\beta = 3, 5, 10$ and $\sigma = 100$. For each entangled resource (associated with a specific plot style), the corresponding curves are ordered from top to bottom with increasing β .

aim, fixing the squeezing parameter at the intermediate value $r = 0.8$, with $n_{th} = 0$, $R^2 = 0.05$, we investigate the behavior of the one-shot fidelities. In Fig. 6, choosing the same values of β and σ as in Fig. 5, we plot \mathcal{F}_{1s} as a function of τ .

Figure 6 shows that the teleportation fidelity remains above the classical threshold up to significantly large values of τ . At $\sigma = 10$ and for small values of the coherent amplitude β (see panel I), the one-shot fidelities associated with the same resource but with different values of β are distinguishable. Vice versa, at $\sigma = 100$ and for larger values of β (see panel II), the fidelities associated with the same resource but different values of β are virtually indistinguishable, and thus effectively β independent. Comparing the performance of the different resources in the time domain, one can distinguish three regimes: For short and long times the one-shot fidelities associated with non-Gaussian resources exhibit a significant enhancement compared to the Gaussian instance, whereas for intermediate times there is a substantial equivalence in the performance of Gaussian and non-Gaussian resources.

VI. CONCLUSIONS

In this article we have investigated the performance of non-Gaussian entangled resources in nonideal protocols of quantum teleportation of input coherent states. We have resorted to the characteristic function formalism for the description of protocols affected by decoherence. We have discussed how the effects of decoherence stemming from photon losses in fiber and imperfect Bell measurements affect the success probability of teleportation. In particular, we have established that, while the fidelities associated with different resources remain above the classical benchmark for quite long times, the non-Gaussian resources always perform better than the Gaussian ones, in the ideal as well as in the nonideal quantum teleportation protocol.

The present analysis should be extended to include teleportation of two-mode states using multimode non-Gaussian resources [45]. It would be also interesting to consider the optimization of teleportation protocols with non-Gaussian entangled resources with respect to local properties (such as

single-mode squeezing), by extending the existing schemes for the local optimization of Gaussian resources [46].

ACKNOWLEDGMENTS

This work has been realized in the framework of the FP7 STREP Project HIP (Hybrid Information Processing). The authors acknowledge financial support from the European Commission of the European Union under the FP7 STREP Project HIP (Hybrid Information Processing), Grant Agreement n. 221889, from MIUR under the FARB funds, from INFN under Iniziativa Specifica PG 62, and from CNR-INFN Research Center Coherentia. One of us (F.I.) acknowledges support from the ISI Foundation for Scientific Interchange.

APPENDIX A: REALISTIC TELEPORTATION PROTOCOL IN THE CHARACTERISTIC FUNCTION REPRESENTATION

Here we outline in some detail the description of the non-ideal BK teleportation protocol in terms of the characteristic function formalism. Let us consider the Bell measurement shown in Fig. 2. The 50-50 beam splitter BS₁ acts on the initial density operator ρ_0 through a SU(2) transformation $U_{BS_1}(\frac{\pi}{4})$, consisting of a balanced mixing of the modes “in” and 1:

$$\rho'_0 = U_{BS_1}\left(\frac{\pi}{4}\right) \rho_0 U_{BS_1}^\dagger\left(\frac{\pi}{4}\right). \quad (\text{A1})$$

This transformation yields the following relation among the phase-space variables corresponding to the input and output modes of the beam splitter:

$$\begin{aligned} x'_{\text{in}} &= \frac{1}{\sqrt{2}}(x_{\text{in}} + x_1), & p'_{\text{in}} &= \frac{1}{\sqrt{2}}(p_{\text{in}} + p_1), \\ x'_1 &= \frac{1}{\sqrt{2}}(x_{\text{in}} - x_1), & p'_1 &= \frac{1}{\sqrt{2}}(p_{\text{in}} - p_1), \end{aligned} \quad (\text{A2})$$

where the canonical variables x'_j and p'_j correspond to the primed modes j' ($j' = \text{in}', 1'$). Using Eq. (A2), the characteristic function χ'_0 associated with the density operator ρ'_0 reads

$$\begin{aligned} \chi'_0(x'_{\text{in}}, p'_{\text{in}}; x'_1, p'_1; x_2, p_2) \\ = \chi_{\text{in}} \left[\frac{1}{\sqrt{2}}(x'_{\text{in}} + x'_1), \frac{1}{\sqrt{2}}(p'_{\text{in}} + p'_1) \right] \\ \times \chi_{\text{res}} \left[\frac{1}{\sqrt{2}}(x'_{\text{in}} - x'_1), \frac{1}{\sqrt{2}}(p'_{\text{in}} - p'_1), x_2, p_2 \right]. \end{aligned} \quad (\text{A3})$$

The fields 1' and in' at the output of the beam splitter BS₁ feed the input ports of the two beam splitters BS₂ and BS₃, respectively, with equal transmissivity η (see Fig. 2). The remaining input ports of the beam splitters are fed with the field modes 3' and 4', initially in the vacuum states $|0\rangle_{4'}$ and $|0\rangle_{3'}$, corresponding to the characteristic functions

$$\chi_k(x'_k, p'_k) = e^{-\frac{1}{4}(x'^2_k + p'^2_k)}, \quad k = 3, 4. \quad (\text{A4})$$

The beam splitters BS₂ and BS₃, associated with the SU(2) transformations $U_{BS_j}(\eta)$ ($j = 2, 3$), transform the variables x'_j and p'_j ($j = \text{in}, 1, 3, 4$) according to the following relations:

$$\begin{aligned} x'_1 &= Tx'_1 - Rx'_4, & p'_1 &= Tp'_1 - Rp'_4, \\ x'_4 &= Tx'_4 + Rx'_1, & p'_4 &= Tp'_4 + Rp'_1, \end{aligned} \quad (\text{A5})$$

$$\begin{aligned} x''_{\text{in}} &= Tx'_{\text{in}} - Rx'_3, & p''_{\text{in}} &= Tp'_{\text{in}} - Rp'_3, \\ x''_3 &= Tx'_3 + Rx'_{\text{in}}, & p''_3 &= Tp'_3 + Rp'_{\text{in}}, \end{aligned} \quad (\text{A6})$$

where $T^2 = \eta$ and $R^2 = 1 - \eta$ denote, respectively, transmissivity and reflectivity of the beam splitters, and double primes denote output modes. At the output of BS₂ and BS₃, the transformed five-mode density operator reads

$$\begin{aligned} \rho_{\text{BS}} &= U_{BS_3}(\eta)U_{BS_2}(\eta)\rho'_0 \times |0\rangle_{3'3'}\langle 0| \\ &\otimes |0\rangle_{4'4'}\langle 0|U_{BS_2}^\dagger(\eta)U_{BS_3}^\dagger(\eta), \end{aligned} \quad (\text{A7})$$

where ρ'_0 is given by Eq. (A1). By exploiting the aforementioned transformations, a simple formal manipulation yields the characteristic function χ_{BS} corresponding to ρ_{BS} :

$$\begin{aligned} \chi_{\text{BS}}(x''_{\text{in}}, p''_{\text{in}}; x''_1, p''_1; x_2, p_2; x''_3, p''_3; x''_4, p''_4) \\ = \chi_{\text{in}} \left(\frac{1}{\sqrt{2}}[Tx''_{\text{in}} + Rx''_3 + Tx''_1 + Rx''_4], \right. \\ \left. \frac{1}{\sqrt{2}}[Tp''_{\text{in}} + Rp''_3 + Tp''_1 + Rp''_4] \right) \\ \times \chi_{\text{res}} \left(\frac{1}{\sqrt{2}}[Tx''_{\text{in}} + Rx''_3 - Tx''_1 - Rx''_4], \right. \\ \left. \frac{1}{\sqrt{2}}[Tp''_{\text{in}} + Rp''_3 - Tp''_1 - Rp''_4]; x_2, p_2 \right) \\ \times \chi_3(Tx''_3 - Rx''_{\text{in}}, Tp''_3 - Rp''_{\text{in}}) \\ \times \chi_4(Tx''_4 - Rx''_1, Tp''_4 - Rp''_1), \end{aligned} \quad (\text{A8})$$

where the functions χ_k , with $k = 3, 4$, are given by Eq. (A4). The Bell measurement, which consists of the two homodyne measurements of the variables p''_{in} and x''_1 , yields the results $p''_{\text{in}} = \tilde{p}$ and $x''_1 = \tilde{x}$ and transforms the characteristic function χ_{BS} to (see appendix B for details)

$$\begin{aligned} \chi_{\text{Bm}}(x_2, p_2) &= \frac{\mathcal{P}^{-1}(\tilde{p}, \tilde{x})}{(2\pi)^2} \int dx''_{\text{in}} dp''_1 e^{ix''_{\text{in}}\tilde{p} - i\tilde{x}p''_1} \\ &\times \chi_{\text{BS}}(x''_{\text{in}}, 0; 0, p''_1; x_2, p_2; 0, 0; 0, 0). \end{aligned} \quad (\text{A9})$$

Here $\mathcal{P}(\tilde{p}, \tilde{x})$ is the distribution function of the outcomes \tilde{p} and \tilde{x} . It reads

$$\begin{aligned} \mathcal{P}(\tilde{p}, \tilde{x}) &= \text{Tr}[|\tilde{p}\rangle_{\text{in}'}\langle \tilde{p}| \otimes |\tilde{x}\rangle_{1'}\langle \tilde{x}| \rho_{\text{BS}}] \\ &= \frac{1}{(2\pi)^2} \int dx''_{\text{in}} dp''_1 \exp\{ix''_{\text{in}}\tilde{p} - i\tilde{x}p''_1\} \\ &\times \chi_{\text{BS}}(x''_{\text{in}}, 0; 0, p''_1; 0, 0; 0, 0; 0, 0). \end{aligned} \quad (\text{A10})$$

Let us notice that in Eq. (A9) the modes 3'' and 4'', associated with the unused output ports of the two fictitious beam splitters, have been traced out. This is equivalent to setting to zero in the function χ_{BS} the variables x''_j and p''_j with $j = 3, 4$. Meanwhile, mode 2 propagates in a noisy channel toward Bob's location. The dynamics of this mode is described by the master equation (3), and the corresponding diffusion equation for the characteristic function $\chi_t(x_2, p_2)$ is [42,43]

$$\begin{aligned} \partial_t \chi_t(x_2, p_2) &= -\frac{\Upsilon}{2} \left[\left(\frac{1}{2} + n_{\text{th}} \right) (x_2^2 + p_2^2) \right. \\ &\left. + x_2 \partial_{x_2} + y_2 \partial_{y_2} \right] \chi_t(x_2, p_2). \end{aligned} \quad (\text{A11})$$

Given the initial characteristic function $\chi_{\text{Bm}}(x_2, p_2)$, Eq. (A9), the global characteristic function $\chi_t(x_2, p_2)$ following the Bell measurement is given by the solution of Eq. (A11):

$$\begin{aligned} \chi_t(x_2, p_2) &= \chi_{\text{Bm}}(e^{-\frac{1}{2}\Upsilon t} x_2, e^{-\frac{1}{2}\Upsilon t} p_2) \\ &\times \exp\left\{-\frac{1}{2}(1 - e^{-\Upsilon t})\left(\frac{1}{2} + n_{\text{th}}\right)(x_2^2 + p_2^2)\right\}. \end{aligned} \quad (\text{A12})$$

After recovering the classical information, Bob performs on mode 2 the displacement $\lambda = g(\tilde{x} + i\tilde{p})$, where g is the gain factor. One easily verifies that, given a state ρ_t described by the characteristic function $\chi_t(x_2, p_2)$, the displaced state $D_2(\lambda)\rho_t D_2^\dagger(\lambda)$ is described by the characteristic function

$$\chi_D(x_2, p_2) = \chi_t(x_2, p_2) e^{i\sqrt{2}\text{Re}[\lambda]p_2 - i\sqrt{2}\text{Im}[\lambda]x_2}. \quad (\text{A13})$$

In order to obtain the density operator ρ_{out} [or, equivalently, the characteristic function $\chi_{\text{out}}(x_2, p_2)$] of the final output state of the teleportation protocol, one must take the average of all the possible outcomes \tilde{x} , \tilde{p} of the Bell measurement:

$$\begin{aligned} \chi_{\text{out}}(x_2, p_2) &= \int d\tilde{x} d\tilde{p} \mathcal{P}(\tilde{p}, \tilde{x}) \chi_D(x_2, p_2) \\ &= \frac{1}{(2\pi)^2} \int d\tilde{x} d\tilde{p} dx''_1 dp''_1 \\ &\times \exp\{i\tilde{x}(\sqrt{2}gp_2 - p''_1) - i\tilde{p}(\sqrt{2}gx_2 - x''_1)\} \\ &\times \chi_{\text{BS}}(x''_1, 0; 0, p''_1; e^{-\frac{1}{2}\Upsilon t} x_2, e^{-\frac{1}{2}\Upsilon t} p_2; 0, 0; 0, 0) \\ &\times \exp\left\{-\frac{1}{2}(1 - e^{-\Upsilon t})\left(\frac{1}{2} + n_{\text{th}}\right)(x_2^2 + p_2^2)\right\}. \end{aligned} \quad (\text{A14})$$

Finally, by exploiting the relation $(2\pi)^{-1} \int dk \exp\{ikx\} = \delta(x)$, and recalling the expression Eq. (A8) of χ_{BS} , we find that Eq. (A14) reduces to Eq. (4).

APPENDIX B: HOMODYNE MEASUREMENT IN THE CHARACTERISTIC FUNCTION REPRESENTATION

In this appendix we describe the homodyne measurement for a multimode state in the characteristic function representation. In particular, we determine the expression for the density operator and for its characteristic function of the reduced state after postselection, that is, of the output state resulting from the homodyne measurements on appropriately selected modes. Let us consider a three-mode quantum state ρ_{123} , with characteristic function $\chi_{123}(\alpha_1, \alpha_2, \alpha_3) = \text{Tr}[\rho_{123} D_1(\alpha_1) D_2(\alpha_2) D_3(\alpha_3)] \equiv \chi_{123}(x_1, p_1; x_2, p_2; x_3, p_3)$, with $\alpha_j = 2^{-1/2}(x_j + ip_j)$ ($j = 1, 2, 3$). Let us recall that ρ_{123} can be written in terms of the Weyl expansion:

$$\begin{aligned} \rho_{123} &= \frac{1}{\pi^3} \int d^2\alpha_1 d^2\alpha_2 d^2\alpha_3 \chi_{123}(\alpha_1, \alpha_2, \alpha_3) \\ &\times D_1(-\alpha_1) D_2(-\alpha_2) D_3(-\alpha_3). \end{aligned} \quad (\text{B1})$$

Homodyne measurements performed on two modes, acting as two conditional measurements, reduce the three-mode state to a single-mode one. Let $p_1 = \tilde{p}$ and $x_2 = \tilde{x}$ be the results of the

homodyne measurements of the quadratures p_1 and x_2 . The homodyne measurements are expressed by projections on the quadrature eigenstates $|\tilde{p}\rangle_1$ and $|\tilde{x}\rangle_2$. Thus the output state $\tilde{\rho}_3$ subsequent to the conditional measurements is

$$\tilde{\rho}_3 = \mathcal{P}^{-1}(\tilde{p}, \tilde{x}) \text{Tr}_{12}[\rho_{123}]_1 \langle \tilde{p} | \otimes \langle \tilde{x} | \rho_{123} \rangle. \quad (\text{B2})$$

Here the normalization factor $\mathcal{P}(\tilde{p}, \tilde{x}) = \text{Tr}_3[\tilde{\rho}_3]$ represents the distribution function of the outcomes \tilde{p} and \tilde{x} . By using the relations

$${}_1\langle \tilde{p} | D_1(-\alpha_1) | \tilde{p} \rangle_1 = e^{-\frac{i}{2}x_1 p_1 + ix_1 \tilde{p}} \delta(p_1), \quad (\text{B3})$$

$${}_2\langle \tilde{x} | D_2(-\alpha_2) | \tilde{x} \rangle_2 = e^{-\frac{i}{2}x_2 p_2 - i\tilde{x} p_2} \delta(x_2), \quad (\text{B4})$$

Eq. (B2) writes

$$\begin{aligned} \tilde{\rho}_3 &= \frac{\mathcal{P}^{-1}(\tilde{p}, \tilde{x})}{(2\pi)^3} \int dx_1 dp_2 dx_3 dp_3 e^{ix_1 \tilde{p} - i\tilde{x} p_2} \\ &\times \chi_{123}(x_1, 0; 0, p_2; x_3, p_3) D_3\left(-\frac{x_3 + ip_3}{\sqrt{2}}\right). \end{aligned} \quad (\text{B5})$$

Denoting by $\chi_3(x_3, p_3)$ the characteristic function of the state $\tilde{\rho}_3$, we have

$$\tilde{\rho}_3 = \frac{1}{2\pi} \int dx_3 dp_3 \chi_3(x_3, p_3) D_3\left(-\frac{x_3 + ip_3}{\sqrt{2}}\right). \quad (\text{B6})$$

Comparing Eqs. (B5) and (B6), we obtain

$$\begin{aligned} \chi_3(x_3, p_3) &= \frac{\mathcal{P}^{-1}(\tilde{p}, \tilde{x})}{(2\pi)^2} \int dx_1 dp_2 e^{ix_1 \tilde{p} - i\tilde{x} p_2} \\ &\times \chi_{123}(x_1, 0; 0, p_2; x_3, p_3). \end{aligned} \quad (\text{B7})$$

Moreover, it is easy to verify that

$$\begin{aligned} \mathcal{P}(\tilde{p}, \tilde{x}) &= \frac{1}{(2\pi)^2} \int dx_1 dp_2 e^{ix_1 \tilde{p} - i\tilde{x} p_2} \\ &\times \chi_{123}(x_1, 0; 0, p_2; 0, 0). \end{aligned} \quad (\text{B8})$$

APPENDIX C: ANALYTICAL EXPRESSIONS FOR THE FIDELITIES

In this appendix we report the analytical expressions for the fidelities of teleportation of input coherent states using two classes of non-Gaussian entangled resources: the squeezed Bell-like states (7) and the squeezed catlike states (8). For comparison we include also the expressions of the fidelities associated with the Gaussian twin beam and of the Buridan donkey state (10). The fidelity $\mathcal{F}_{\text{SB}}^{(g)}(r, \delta)$ for the squeezed Bell-like state ((7) reads

$$\begin{aligned} \mathcal{F}_{\text{SB}}^{(g)}(r, \delta) &= \frac{4}{\Delta} e^{-\frac{4}{\Delta}(\tilde{g}-1)^2|\beta|^2} \left(1 + \frac{2e^{-4r-2\tau}}{\Delta^4}\right. \\ &\times [(1 + e^{\frac{5}{2}\tilde{g}})^2 - e^{4r}(1 - e^{\frac{5}{2}\tilde{g}})^2]^2 \\ &\times [\Delta^2 - 8\Delta(\tilde{g}-1)^2|\beta|^2 + 8(\tilde{g}-1)^4|\beta|^4] \sin^2 \delta \\ &+ \frac{2e^{-2r-\tau}}{\Delta^2} [4(\tilde{g}-1)^2|\beta|^2 - \Delta] \sin \delta \{\cos \delta \\ &\times [-(1 + e^{\frac{5}{2}\tilde{g}})^2 + e^{4r}(1 - e^{\frac{5}{2}\tilde{g}})^2] + \sin \delta \\ &\times [(1 + e^{\frac{5}{2}\tilde{g}})^2 + e^{4r}(1 - e^{\frac{5}{2}\tilde{g}})^2]\} \Big), \end{aligned} \quad (\text{C1})$$

where

$$\Delta \doteq e^{-2r-\tau}[(1 + e^{\frac{\tau}{2}}\tilde{g})^2 + e^{4r}(1 - e^{\frac{\tau}{2}}\tilde{g})^2 + 2e^{2r+\tau}(1 + \tilde{g}^2 + 2\Gamma_{\tau,R})], \quad (\text{C2})$$

$$\tilde{g} = gT, \quad (\text{C3})$$

and $\Gamma_{\tau,R}$ is defined in Eq. (5). The fidelity $\mathcal{F}_{\text{SC}}^{(g)}(r, \delta, |\gamma\rangle)$ for the squeezed catlike state (8) reads

$$\begin{aligned} \mathcal{F}_{\text{SC}}^{(g)}(r, \delta, |\gamma\rangle) &= \frac{4}{\Delta(1 + e^{-|\gamma|^2} \sin 2\delta)} (\cos^2 \delta \\ &\times e^{-\frac{4}{\Delta}(\tilde{g}-1)^2|\beta|^2} + e^{-|\gamma|^2 - \frac{1}{\Delta}[(\tilde{g}-1)(\beta+\beta^*) - e^r \tilde{g}|\gamma|^2]} \\ &\times \sin \delta \cos \delta \{e^{\frac{1}{\Delta}[(\tilde{g}-1)(\beta-\beta^*) + e^{-r} \tilde{g}|\gamma|^2]} + \text{c.c.}\} \\ &+ \sin^2 \delta e^{-\frac{4}{\Delta}(\tilde{g}-1)\beta - e^r |\gamma|(\tilde{g} - e^{\frac{\tau}{2}})^2}). \end{aligned} \quad (\text{C4})$$

For $\tilde{g} = 1$ and $\tau = R = n_{\text{th}} = 0$, Eqs. (C1) and (C4) reduce to the expressions of the fidelities associated with the ideal protocol with unit gain, which had been originally determined in Ref. [27]. By letting $\delta = 0$ in Eqs. (C1) and (C4), we recover

the fidelity $\mathcal{F}_{\text{TWB}}^{(g)}(r)$ associated with the Gaussian twin-beam resource:

$$\mathcal{F}_{\text{TWB}}^{(g)}(r) = \frac{4}{\Delta} e^{-\frac{4}{\Delta}(\tilde{g}-1)^2|\beta|^2}. \quad (\text{C5})$$

Let us notice that such a result can also be obtained by putting $|\gamma| = 0$ in Eq. (C4). For completeness, we also report the expression of the teleportation fidelity associated with the Buridan donkey entangled resource (10):

$$\begin{aligned} \mathcal{F}_{\text{SB2}}^{(g)}(r, \delta) &= \frac{4}{\Delta} e^{-\frac{4}{\Delta}(\tilde{g}-1)^2|\beta|^2} \left(1 + \frac{e^{-2r-\tau}}{\Delta^2} \right. \\ &\times \{[(1 + e^{\frac{\tau}{2}}\tilde{g})^2 + e^{4r}(1 - e^{\frac{\tau}{2}}\tilde{g})^2] \\ &\times [4(\tilde{g} - 1)^2|\beta|^2 - \Delta] + 2 \cos 2\delta e^{2r}(e^{\tau}\tilde{g}^2 - 1) \\ &\times [\Delta - 4(\tilde{g} - 1)^2|\beta|^2] - 2 \sin 2\delta (\tilde{g} - 1)^2 \\ &\times (\beta^2 + \beta^{*2})[(1 + e^{\frac{\tau}{2}}\tilde{g})^2 - e^{4r}(1 - e^{\frac{\tau}{2}}\tilde{g})^2]\} \Big). \end{aligned} \quad (\text{C6})$$

-
- [1] F. Dell'Anno, S. De Siena, and F. Illuminati, *Phys. Rep.* **428**, 53 (2006).
- [2] M. S. Kim, W. Son, V. Buřek, and P. L. Knight, *Phys. Rev. A* **65**, 032323 (2002).
- [3] A. Kitagawa, M. Takeoka, M. Sasaki, and A. Chefles, *Phys. Rev. A* **73**, 042310 (2006).
- [4] V. V. Dodonov and L. A. de Souza, *J. Opt. B: Quantum Semiclass. Opt.* **7**, S490 (2005).
- [5] N. J. Cerf, O. Krüger, P. Navez, R. F. Werner, and M. M. Wolf, *Phys. Rev. Lett.* **95**, 070501 (2005).
- [6] G. Adesso, F. Dell'Anno, S. De Siena, F. Illuminati, and L. A. M. Souza, *Phys. Rev. A* **79**, 040305(R) (2009).
- [7] T. Tyc and N. Korolkova, *New J. Phys.* **10**, 023041 (2008).
- [8] G. S. Agarwal and K. Tara, *Phys. Rev. A* **43**, 492 (1991).
- [9] G. Bjork and Y. Yamamoto, *Phys. Rev. A* **37**, 4229 (1988).
- [10] Z. Zhang and H. Fan, *Phys. Lett. A* **165**, 14 (1992).
- [11] M. Dakna, T. Anhut, T. Opatrny, L. Knöll, and D. G. Welsch, *Phys. Rev. A* **55**, 3184 (1997).
- [12] M. S. Kim, E. Park, P. L. Knight, and H. Jeong, *Phys. Rev. A* **71**, 043805 (2005).
- [13] D. Menzies and R. Filip, *Phys. Rev. A* **79**, 012313 (2009).
- [14] A. Zavatta, S. Viciani, and M. Bellini, *Science* **306**, 660 (2004).
- [15] A. I. Lvovsky and S. A. Babichev, *Phys. Rev. A* **66**, 011801(R) (2002).
- [16] J. Wenger, R. Tualle-Brouiri, and P. Grangier, *Phys. Rev. Lett.* **92**, 153601 (2004).
- [17] A. Ourjoumtsev, A. Dantan, R. Tualle-Brouiri, and P. Grangier, *Phys. Rev. Lett.* **98**, 030502 (2007).
- [18] V. Parigi, A. Zavatta, M. Kim, and M. Bellini, *Science* **317**, 1890 (2007).
- [19] A. Ourjoumtsev, H. Jeong, R. Tualle-Brouiri, and P. Grangier, *Nature (London)* **448**, 784 (2007).
- [20] M. M. Wolf, G. Giedke, and J. I. Cirac, *Phys. Rev. Lett.* **96**, 080502 (2006).
- [21] T. Opatrny, G. Kurizki, and D.-G. Welsch, *Phys. Rev. A* **61**, 032302 (2000).
- [22] P. T. Cochrane, T. C. Ralph, and G. J. Milburn, *Phys. Rev. A* **65**, 062306 (2002).
- [23] S. Olivares, M. G. A. Paris, and R. Bonifacio, *Phys. Rev. A* **67**, 032314 (2003).
- [24] F. Dell'Anno, S. De Siena, L. Albano, and F. Illuminati, *Phys. Rev. A* **76**, 022301 (2007).
- [25] Y. Yang and F.-L. Li, *Phys. Rev. A* **80**, 022315 (2009).
- [26] M. G. Genoni, M. G. A. Paris, and K. Banaszek, *Phys. Rev. A* **76**, 042327 (2007); **78**, 060303(R) (2008).
- [27] F. Dell'Anno, S. De Siena, L. Albano Farias, and F. Illuminati, *Eur. Phys. J. Special Topics* **160**, 115 (2008).
- [28] R. J. Glauber, *Phys. Rev. A* **131**, 2766 (1963).
- [29] A. Vukics, J. Janszky, and T. Kobayashi, *Phys. Rev. A* **66**, 023809 (2002).
- [30] A. V. Chizhov, L. Knöll, and D.-G. Welsch, *Phys. Rev. A* **65**, 022310 (2002); A. V. Chizhov, *JETP Lett.* **80**, 711 (2004).
- [31] P. Marian and T. A. Marian, *Phys. Rev. A* **74**, 042306 (2006).
- [32] W. P. Bowen, N. Treps, B. C. Buchler, R. Schnabel, T. C. Ralph, T. Symul, and P. K. Lam, *IEEE J. Sel. Top. Quant.* **9**, 1519 (2003).
- [33] T. Ide, H. F. Hofmann, A. Furusawa, and T. Kobayashi, *Phys. Rev. A* **65**, 062303 (2002).
- [34] P. T. Cochrane and T. C. Ralph, *Phys. Rev. A* **67**, 022313 (2003).
- [35] S. L. Braunstein and H. J. Kimble, *Phys. Rev. Lett.* **80**, 869 (1998).
- [36] S. J. van Enk, *Phys. Rev. A* **60**, 5095 (1999).
- [37] A. Vukics, J. Janszky, and T. Kobayashi, *Phys. Rev. A* **66**, 023809 (2002).
- [38] H. F. Hofmann, T. Ide, T. Kobayashi, and A. Furusawa, *Phys. Rev. A* **62**, 062304 (2000).
- [39] A. Furusawa and N. Takei, *Phys. Rep.* **443**, 97 (2007).
- [40] P. van Loock, *Fortschr. Phys.* **50**, 12 (2002).

- [41] U. Leonhardt and H. Paul, *Phys. Rev. A* **48**, 4598 (1993).
- [42] D. Walls and G. Milburn, *Quantum Optics* (Springer, Berlin, 1994).
- [43] A. Serafini, M. G. A. Paris, F. Illuminati, and S. De Siena, *J. Opt. B: Quantum Semiclass. Opt.* **7**, R19 (2005).
- [44] S. L. Braunstein, C. A. Fuchs, and H. J. Kimble, *J. Mod. Opt.* **47**, 267 (2000); K. Hammerer, M. M. Wolf, E. S. Polzik, and J. I. Cirac, *Phys. Rev. Lett.* **94**, 150503 (2005).
- [45] S. Adhikari, A. S. Majumdar, and N. Nayak, *Phys. Rev. A* **77**, 012337 (2008).
- [46] G. Adesso and F. Illuminati, *Phys. Rev. Lett.* **95**, 150503 (2005); A. Mari and D. Vitali, *Phys. Rev. A* **78**, 062340 (2008).